Time-Marching Transonic Flutter Solutions Including Angle-of-Attack Effects

John W. Edwards,* Robert M. Bennett,† Woodrow Whitlow Jr.,† and David A. Seidel†
NASA Langley Research Center, Hampton, Virginia

Transonic aeroelastic solutions based upon the transonic small perturbation potential equation are studied. Time-marching transient solutions of plunging and pitching airfoils are analyzed using a complex exponential modal identification technique. The HYTRAN2 code is used to determine transonic flutter boundaries vs Mach number and angle of attack for NACA 64A010 and MBB A-3 airfoils. In that code, a monotone differencing method, which eliminates leading edge expansion shocks, is used to solve the potential equation. When the effect of static pitching moment upon the angle of attack is included, the MBB A-3 airfoil can have multiple flutter speeds at a given Mach number.

Nomenclature

a = nondimensional elastic axis location, measured from midchord
a_i = amplitude of ith mode, Eq. (10)
A,B = (4×4) and (4×2) matrices, Eq. (4)
b = airfoil semichord, m
c_ℓ = nondimensional lift coefficient, positive downwards
c_m = nondimensional moment coefficient about a, positive nose up
C_p = nondimensional pressure coefficient
$f(x,t)$ = airfoil shape function
h = nondimensional plunge displacement of elastic axis, positive downwards
I = identity matrix
j = $\sqrt{-1}$
k = reduced frequency, $\omega b/U$
k_α = pitch spring constant
m = airfoil mass per unit span
M = Mach number
M,K,B' = (2×2) mass, stiffness, and input matrices, Eq. (3)
r_α = radius of gyration about elastic axis
s_i = $\sigma_i + j\omega_i$ = Laplace transform variable, rad/s
t,τ = time, s
T = integration step size, s
U = airspeed, m/s
$\boldsymbol{u}$ = (2×1) airload vector, Eq. (3)
V = speed index, $U/b\omega_\alpha\sqrt{\mu}$
x,z = Cartesian coordinates
$\boldsymbol{x}$ = (4×1) state vector, Eq. (4)
x_α = dimensionless static unbalance
$\boldsymbol{y}$ = (2×1) mode vector, Eq. (3)
α = angle of attack, rad (deg)
γ = ratio of specific heats
ζ_i = σ_i/ω_i = damping ratio of the ith mode
θ = (4×4) matrix, integral of Φ
μ = airfoil mass ratio, $m/\pi\rho b^2$ fluid density, kg/m³
ψ_i = phase of ith mode, Eq. (10)
ϕ = velocity potential
Φ = (4×4) state transition matrix
ω_h,ω_α = uncoupled plunge and pitch mode frequencies, rad/s

Superscripts

T = transpose
$(\dot{})$ = time derivative

Subscripts

f = flutter
i = index
n = time step index
o = initial or steady condition
∞ = freestream

Presented as Paper 82-0685 at the AIAA/ASME/ASCE 23rd Structures, Structural Dynamics and Materials Conference, New Orleans, La., May 10-12, 1982; submitted May 28, 1982; revision received April 11, 1983. This paper is declared a work of the U.S. Government and therefore is in the public domain.

*Aerospace Engineer, Head, Unsteady Aerodynamics Branch. Member AIAA.
†Aerospace Engineer, Unsteady Aerodynamics Branch. Member AIAA.

Introduction

THE calculation of aeroelastic response characteristics in the transonic speed range is of much current interest since the avoidance of transonic flutter is a key design problem. Prior to the development of computer programs capable of solving transonic aerodynamic problems, linear subsonic and supersonic solutions were extended into this regime even though the assumptions of the underlying theory were violated. The LTRAN2[1] computer program solves the two-dimensional, low-frequency, transonic, small perturbation potential equation. Its application to a simple aeroelastic stability problem was demonstrated by Ballhaus and Goorjian.[2] Reference 2 illustrates the two approaches which have been followed in the application of transonic aerodynamic calculations to aeroelasticity; namely, harmonic analysis and time-marching analysis. The former assumes that the unsteady aerodynamic forces are locally linear and utilizes traditional modal superposition of harmonic loads while the latter delays the question of linearity by calculating the transient response of the coupled aerodynamic-structural system. If the assumption of local linearity is warranted, the harmonic analysis approach may offer a significant computational savings. Rizzetta[3] examined the time-marching technique, using the LTRAN2 code, to calculate the unsteady airloads. The initial conditions chosen were large enough that significant nonlinear effects occurred in the calculated unsteady airloads, indicating large shock motions. Yang et al.[4] also studied a time-marching scheme and compared harmonic flutter analyses[5] using oscillatory airloads derived from LTRAN2 and UTRANS2.[6]

Since the original LTRAN2 code is accurate only at low frequencies ($k<0.075$), several improvements were made to increase its range of applicability. Houwink and van der Vooren[7] studied the effect of retaining the time-derivative

terms in the boundary and auxiliary conditions in their LTRAN2-NLR code and claimed accuracy to $k=0.4$. Rizzetta and Chin[8] retained, in addition, the high-frequency (ϕ_{tt}) term in the governing equation. Isogai[9] has included both of these effects in a computer code which has been used to generate oscillatory airloads for a harmonic flutter analysis of a two-dimensional airfoil section. The analysis demonstrated a significant transonic dip in the section's flutter boundary. Borland and Rizzetta[10] have developed a three-dimensional unsteady aerodynamic code, XTRAN3S, and have utilized a centered-difference structural integration technique to obtain transient time-marching flutter solution.

Application of these time-dependent small perturbation codes has been hampered by numerical stability problems which occur for large amplitude motion and/or large angles of attack. The current study modifies the LTRAN2-NLR code with the monotone differencing scheme of Engquist and Osher[11] in order to eliminate the source of this problem, namely expansion shocks near the airfoil leading edge. The resulting code is termed HYTRAN2. This code has been used to study the accuracy and stability of the various numerical integration techniques which may be used in transient time-marching calculations.[12] The accuracy of the finite difference codes may be established using recent analytic solutions by Bland[13] of the linearized LTRAN2, HYTRAN2, and EXTRAN2 aerodynamic problems. The linearized version of the HYTRAN2 code is then used to investigate the accuracy of various numerical integration techniques for the structural equations of motion. A comparison is made of transonic flutter boundaries of the NACA 64A010 airfoil calculated by four nonlinear transonic codes. The effect of angle of attack upon the flutter boundaries of the NACA 64A010 and the MBB A-3 airfoils is also demonstrated. Finally, the effect upon the flutter boundary of including the aeroelastic twisting resulting from the steady pitching moment is demonstrated.

Unsteady Transonic Small Perturbation Equation

The calculations described herein were obtained from a modified version of the LTRAN2-NLR code[7] which solves the low-frequency transonic small perturbation (TSP) potential equation

$$[1-M_\infty^2-(\gamma^*+1)M_\infty^2\phi_x]\phi_{xx}+\phi_{zz}-2M_\infty^2\phi_{xt}=0 \qquad (1)$$

where $\gamma^*=2-(2-\gamma)M_\infty^2$. The airfoil boundary and wake conditions are

$$\phi_z=f_x+f_t \qquad z=\pm 0, \quad 0<x<1 \qquad (2a)$$

$$[\phi_x]+[\phi_t]=0 \qquad z=0, \quad x>1 \qquad (2b)$$

where the airfoil coordinates are given by $z=f(x,t)$. Aerodynamic loads are given in terms of a nondimensional pressure coefficient, C_p, which in the small perturbation limit becomes

$$C_p=-2(\phi_x+\phi_t) \qquad (2c)$$

The original LTRAN2[1] grid of 99×79 points in the x and z directions, respectively, with 33 points on the airfoil chord was used. The original LTRAN2-NLR and LTRAN2 codes are very sensitive to angle-of-attack changes and large airfoil pitching or plunging motions, and numerical instabilities generated at the leading edge[14] can lead to program failure. The monotone differencing method of Engquist and Osher[11] eliminates the leading-edge expansion shocks which cause this problem and has been incorporated into a code termed HYTRAN2 which was used for this study. Solutions obtained with the time-derivative terms of Eqs. (2) deleted are referred to as LTRAN2 solutions, while solutions with a $-M_\infty^2\phi_{tt}$ term added to Eq. (1) are referred to as EXTRAN2 solutions. References 8 and 9 give results obtained from EXTRAN2 type codes.

The frequency limits of LTRAN2 and HYTRAN2 codes are generally accepted as $k\approx 0.075$ and $k\approx 0.4$, respectively. These estimates are based upon comparisons of results from linearized versions of these finite difference codes [obtained by deleting the $\phi_x\phi_{xx}$ term in Eq. (1)] with classical solutions of the subsonic wave equation. This has left open the questions of convergence of solutions for a given grid and accuracy of the solutions. Bland[13] has modified the kernel function of the Possio integral equation to enable computation of exact analytic solutions of the LTRAN2 and HYTRAN2 linearized problems. Figure 1 gives comparisons of his exact c_{ℓ_α} solutions at $M=0.8$ for the three different kernels with LTRAN2 and HYTRAN2 results for reduced frequencies up to 0.5. The finite difference results were obtained using three cycles of time-marching calculations with 360 steps/cycle. The agreement between the finite difference and analytical solutions indicates that the finite difference code is quite accurate for the grid and step size used. Also, the departure of LTRAN2 from the analytic EXTRAN2 results above $k\approx 0.05$ confirms the limitations of LTRAN2 mentioned above. The HYTRAN2 results are in better agreement with EXTRAN2 and show a more gradual departure from EXTRAN2. The selection of an upper-frequency limit on HYTRAN2 is somewhat arbitrary.

Time-Marching Aeroelastic Solutions

The classical description of a two-dimensional, pitching and plunging airfoil is assumed. The airfoil lies between ± 1 on the x axis; plunge h, and lift coefficient c_ℓ, are measured positive downwards at the elastic axis a; and pitch α, and moment coefficient about a, c_m, are positive nose up. The equations of motion are written in vector notation as

$$y=M^{-1}Ky+M^{-1}B'u \qquad (3)$$

where $y^T=[h\alpha]$, $u^T=[(c_\ell-c_{\ell_o})\ (c_m-c_{m_o})]$, and

$$M=\begin{bmatrix} 1 & x_\alpha \\ x_\alpha & r_a^2 \end{bmatrix}, \quad K=\begin{bmatrix} -\omega_h^2 & 0 \\ 0 & -r_\alpha^2\omega_\alpha^2 \end{bmatrix}$$

$$B'=\frac{\omega_\alpha^2}{\pi}V^2\begin{bmatrix} 1 & 0 \\ 0 & 1 \end{bmatrix}$$

The static load coefficients, c_{ℓ_o} and c_{m_o}, are subtracted from the total coefficients during the time-marching calculation. Thus h and α represent perturbations about assumed static operating conditions. The static angle of attack is a separate input to HYTRAN2 and contributes to f_x in Eq. (2a). The

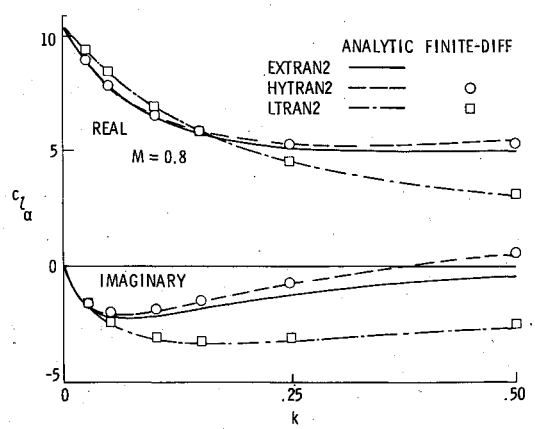

Fig. 1 Comparison of analytic and finite difference calculations of lift coefficient due to pitching oscillation about midchord.

speed index $V=U/b\omega_\alpha\sqrt{\mu}$ determines the density (altitude) assumed for a calculation. As V increases from zero, transient responses are initially damped. Further increases in V will usually lead to neutrally stable oscillations characterizing a flutter boundary. The value of V at flutter is termed the flutter speed index V_f. A fourth-order linear state equation may be developed from Eq. (3) as

$$\dot{x}=Ax+Bu \tag{4}$$

where

$$x^T=[y^T\dot{y}^T]=[h\alpha\dot{h}\dot{\alpha}]$$

and

$$A=\begin{bmatrix}0 & I\\ M^{-1}K & 0\end{bmatrix},\quad B=\begin{bmatrix}0\\ M^{-1}B'\end{bmatrix}$$

Structural Integration Technique

Published studies of time-marching aeroelastic solutions have coupled the structural equations of motion to aerodynamic codes using a variety of numerical integration techniques. Rizzetta[3] used an Adams-Moulton predictor-corrector scheme. Reference 4 reports an algorithm based upon an assumed linear variation of acceleration while a centered-difference integration technique was used in Ref. 10. None of these approaches takes advantage of the linear structure of Eq. (4).

Since Eq. (4) is a finite dimensional linear differential equation, its solution[15] is

$$x(t)=\Phi(t)x(0)+\int_0^t \exp[A(t-\tau)]Bu(\tau)\,d\tau \tag{5}$$

The state transition matrix $\Phi(t)\equiv\exp[At]$ may be calculated to any desired accuracy as the sum of the first n terms of the series expansion of the matrix exponential function. The first term in Eq. (5) is the homogeneous response portion of Eq. (4) while the second term is a convolution integral giving the forced response. For use as a structural integrator in aeroelastic time-marching solutions, Eq. (5) is rewritten to reflect the evolution of the structural state from time step n to time step $n+1$,

$$x[(n+1)T]=\Phi(T)x(nT)$$
$$+\int_{nT}^{(n+1)T}\exp[A((n+1)T-\tau)]Bu(\tau)\,d\tau \tag{6}$$

where T is the step size.

The alternating-direction implicit solution algorithm used in HYTRAN2 requires three pieces of data to calculate the flowfield potential, ϕ_{n+1}, at time step $n+1$: 1) ϕ_n, the potential at time n; 2) x_n, the boundary condition at time n; and 3) x_{n+1}, the boundary condition at time $n+1$. Since the lift and moment are not known over the interval $nT<t<(n+1)T$, the integral in Eq. (6) must be approximated. The simplest approximation is to assume that $u(t)=u(nT)$ over the interval. Then $Bu(nT)$ may be taken out of the integral and a slight change of notation gives

$$x_{n+1}=\Phi x_n+\theta Bu_n \tag{7}$$

where the integral of the transition matrix is

$$\theta=\int_0^T \exp[A(T-\tau)]\,d\tau \tag{8}$$

An improvement upon this approximation may be obtained by considering u to vary linearly between u_n and u_{n+1} in Eq. (6). Then, for small time steps T, the integral is nearly equal to $\theta B(u_{n+1}+u_n)/2$. However, u_{n+1} is not available at this step of the algorithm and an estimate of $u_{n+1}\approx u_n+(u_n-u_{n-1})$ will be used. The resulting algorithm is

$$x_{n+1}=\Phi x_n+\theta B(3u_n-u_{n-1})/2 \tag{9}$$

The integration matrices Φ and θ were calculated using the program described in Ref. 16. The results presented were obtained from transient responses calculated using Eq. (9) for the structural integrator.

Reference 12 describes a numerical evaluation of seven alternative structural integration algorithms. The integration technique given by Eq. (9) was shown to be superior to the others in terms of stability and accuracy. After the steady-state flowfield for the static angle of attack was obtained, the transient was excited by a 1% chord displacement initial condition on the plunge coordinate. The transient was calculated for 250 time steps which yielded 3-6 cycles of oscillation of the dominant flutter mode for the examples studied. To determine a flutter point, several transients were calculated for a range of speed indices, V. Typically, speed indices were used which gave slightly subcritical damped response and slightly supercritical diverging response. The flutter speed index was then determined by interpolation. Once the general nature of the flutter boundary was understood, additional flutter points could generally be obtained in this manner with the calculation of two responses per flutter point.

Section Structural Parameters

The structural parameters for the example studied are: $a=-2$, $x_\alpha=1.8$, $r_\alpha^2=3.48$, $\mu=60$, $\omega_h=100$ rad/s, and $\omega_\alpha=100$ rad/s. The wind-off coupled plunge and pitch frequencies are 71.34 and 533.8 rad/s. This example is the same as case A of Isogai[9,17] which was selected to have plunging and pitching normal modes similar to those of a streamwise section near the wing tip of a sweptback wing. The pivotal point for the plunging mode is 1.44 chordlengths ahead of the leading edge and for the pitching mode it is 0.068 chordlengths ahead of midchord. Isogai[17] has shown a

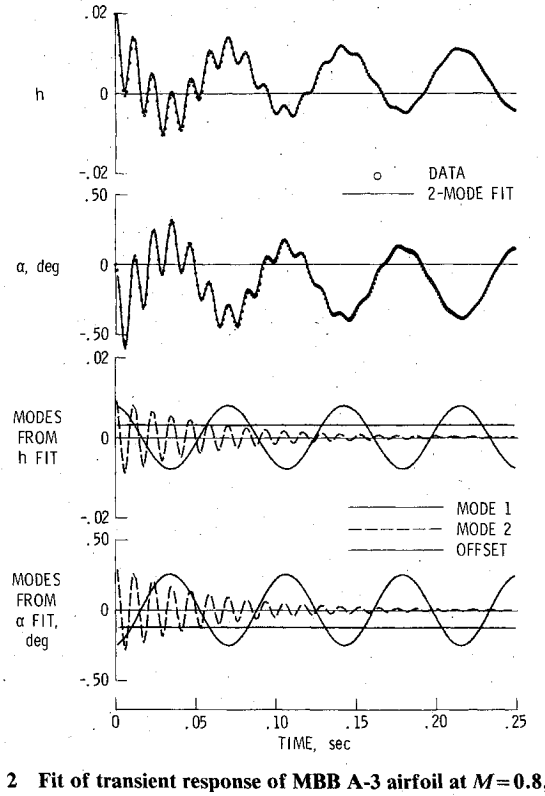

Fig. 2 Fit of transient response of MBB A-3 airfoil at $M=0.8$, $\alpha=0$ deg, and $V_f=0.645$.

significant transonic dip in the flutter speed index of this section with the plunging mode becoming the flutter mode at frequencies ranging from 80-150 rad/s.

Modal Identification Technique

To efficiently use the information contained in the transients, the least squares curve fitting program of Bennett and Desmarais[18] was used. Both h and α responses were fit independently by the function

$$Y(t) = a_0 + \sum_{i=1}^{m} e^{-\sigma_i t} a_i \cos(\omega_i t + \psi_i) \qquad (10)$$

For the two degree-of-freedom example treated, m was set equal to 2. The complex modes thus obtained, $s_i = \sigma_i + j\omega_i$, are estimates of the eigenvalues of the aeroelastic system and can be plotted as a function of speed index, V, giving s plane root loci of the coupled plunge and pitch modes. Figure 2 gives a typical transient response of the MBB A-3 airfoil at $M = 0.8$ and an angle of attack $\alpha = 0$. Shown at the top of the figure are the h and α responses and the fits of the responses. At the bottom of the figure, the time histories of the component modes of the fits are shown. The fits are very good and indicate that nonlinear effects are very small.

Table 1 gives the estimates of the two modes for each of two response time histories. Standard deviations of the estimates are computed from the residuals and are given in brackets beneath the estimates. The estimates given by the independent fits are very consistent with each other although the standard deviations are somewhat optimistic. These results indicate that locally linear techniques are applicable for this case involving plunging oscillations of ± 0.008 semichords and angle-of-attack oscillations of ± 0.25 deg.

Airfoils

Figure 3 shows the profiles of the two airfoils studied. Coordinates for the NACA 64A010 symmetrical airfoil were taken from Abbott and von Doenhoff[19] and for the MBB A-3 supercritical airfoil from Bland.[20] Applications of TSP codes to both airfoils have been extensively reported (e.g., Refs. 3, 8, 21, and 22 for the NACA 64A010 and Refs. 22 and 23 for the MBB A-3). The MBB A-3 theoretical design condition is $M = 0.765$, $\alpha = 1.3$ deg, and $c_\ell = 0.58$, and experimental pressure distributions are given by Bucciantini et al.[24] The airfoil slopes required by HYTRAN2 were generated using the geometry processor of LTRAN2.[1]

Results and Discussion

In this section, flutter boundaries are presented for the structural dynamic model described above and for NACA 64A010 and MBB A-3 airfoils. Steady-pressure distributions for the ranges of Mach number and angle of attack investigated are given in Figs. 4 and 5. In the cases where the steady shocks are located near the trailing edge, the shock strengths are of concern. For these cases, Figs. 4 and 5, the computed Mach numbers ahead of the upper-surface shocks are only slightly less than 1.3—the Mach number at which entropy rises start to become significant indicating that these calculations are on the edge of and possibly outside the range of applicability of TSP theory. At $\alpha = -1.50$ deg, the Mach number on the lower surface of the MBB A-3 is such that these cases may be beyond the scope of the TSP theory.

Table 1 Modal estimates for MBB A-3 response at $M = 0.8$ and $\alpha = 0$ deg

	s_1, rad/s	s_2, rad/s
h fit	$-0.12 + j86.91$	$-17.24 + j535.54$
	$(0.05 + j0.05)$	$(0.31 + j0.32)$
α fit	$-0.02 + j86.74$	$-17.94 + j536.81$
	$(0.07 + j0.07)$	$(0.42 + j0.43)$

Table 2 Modal estimates for NACA 64A010 at $M = 0.8$, $\alpha = 0$ deg, and $V_f = 1.07$ as a function of T

T, s	s_1, rad/s	s_2, rad/s
0.0001	$0.11 + j115.21$	$-31.89 + j536.26$
0.0005	$0.08 + j115.09$	$-32.95 + j536.17$
0.001	$0.02 + j115.18$	$-35.76 + j537.04$
0.002	$-0.08 + j115.54$	$-42.03 + j544.83$
0.003	$-0.07 + j116.08$	$-46.07 + j551.90$

Effect of Integration Step Size

The effect of integration step size upon the modes identified from the angle-of-attack response is given in Table 2 for the NACA 64A010 at $M = 0.8$. The flutter speed index is $V_f = 1.07$, and $k_f = 0.139$. The variation of the modal estimates with step size is slightly smaller than the corresponding variations reported in Ref. 12 for the linearized case. This provides confidence in the application of the time-marching technique to the nonlinear aeroelastic problem.

Effect of Amplitude

The effect of amplitude on the response at flutter was studied for the MBB A-3 airfoil at three conditions:

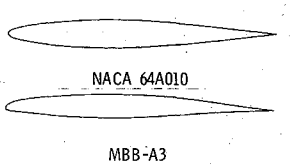

Fig. 3 Airfoil profiles.

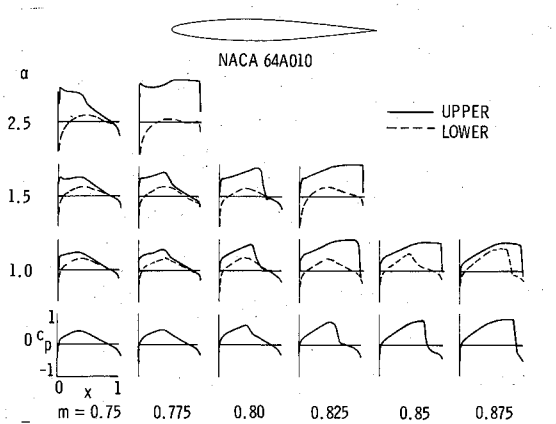

Fig. 4 NACA 64A010 steady pressure distributions as a function of Mach number and angle of attack.

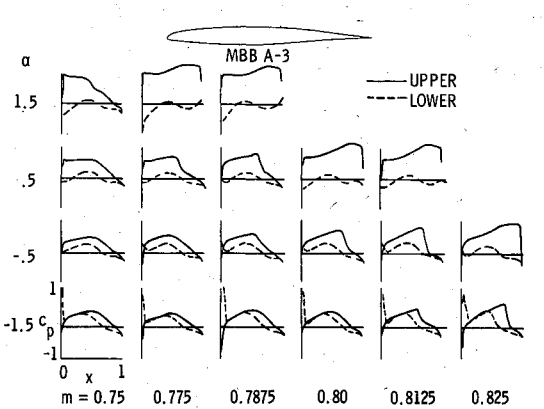

Fig. 5 MBB A-3 steady pressure distributions as a function of Mach number and angle of attack.

1) $M=0.775$ and $\alpha=0$ deg where the flow is subcritical, 2) $M=0.794$ and $\alpha=0.5$ deg where there is a strong shock aft of midchord, and 3) $M=0.8$ and $\alpha=0.5$ deg where the shock is at the trailing edge. Table 3 gives the modal estimates including the amplitude estimates from the α fit for $M=0.775$ which are typical. The flutter speed index is $V_f=1.21$, and $k_f=0.125$. There is a surprisingly small effect of amplitude upon the damping of the flutter mode. The damping ratio ζ changes from $+0.011$ for $h_o=0.01$ where the oscillation amplitude is ± 0.28 deg, to -0.004 for $h_o=0.10$ where the oscillation amplitude is ± 2.97 deg. Inspection of the pressure distribution for the $h_o=0.1$ case during a cycle of oscillation revealed a complex pattern of shock motion. During a portion of the cycle, a strong shock forms near the 70% chord position, travels forward, weakens, and disappears between 40-50% chord. This is the type B shock motion studied by Tijdeman.[25] Also, during the nose-down portion of the cycle a strong shock forms at 5-10% chord on the lower surface. It is interesting that the modal amplitudes a_i are nearly linear with respect to h_o, even for the large amplitudes studied. At $M=0.794$ the effect of amplitude upon the flutter mode was smaller than that shown in Table 3; the change in the flutter root in going from $h_o=0.01$ to 0.10 being $s=-0.30+j0.69$ rad/s. At $M=0.8$ the corresponding change was $s=-1.41-j0.19$. In all cases the standard deviations of the estimates, which did not vary appreciably with h_o, were small and of the order given in Table 2, and the amplitudes varied nearly linearly with h_o. Calculations of amplitude effects were made for the NACA 64A010 and similar small effects on the modal estimates were observed. These results contrast with Dowell et al.[26] who studied forced oscillations of the NACA 64A006 airfoil using LTRAN2 and postulated that nonlinear aerodynamics would be important at $k=0.1$ for oscillatory amplitudes greater than 0.5 deg. In summary, it appears that, for a given Mach number and steady angle of attack, the aeroelastic response of airfoils with dynamics similar to those studied may be treated as locally linear in amplitude within the limits of small disturbance theory.

Comparison of TSP Flutter Boundaries

The transonic flutter boundary of an NACA 64A010 airfoil at $\alpha=0$ deg has been studied by Isogai[9,17] using an EXTRAN2 code to obtain harmonic perturbation airloads and by Ehlers and Weatherill[27] using a transonic code, OPTRAN2, to compute the harmonic linear perturbation airloads. The flutter boundaries in both studies were then calculated using traditional frequency-domain techniques. The comparison of these flutter boundaries with that obtained from time-marching solutions using HYTRAN2 is shown in Fig. 6. Also shown are two flutter points at Mach 0.8 and 0.825 which used LTRAN2 aerodynamics. The LTRAN2 flutter point is conservative by up to 50% in flutter speed index while the HYTRAN2 results are slightly unconservative below $M=0.85$ when compared to EXTRAN2. The HYTRAN2 results compare favorably with Isogai's EXTRAN2 results with both giving minimum flutter speed indices of $V_f\approx 0.5$. The HYTRAN2 and EXTRAN2 curves are displaced from each other by $M\approx 0.015$ which may be due to differences in steady pressure distribution caused by grid differences. The minimum V_f obtained using HYTRAN2 occurs at $M=0.85$ where the steady shock is at $x/2b\approx 0.75$. The flutter speed index is slightly greater at $M=0.875$ where Isogai was unable to obtain a flutter solution. The OPTRAN2 results (using NACA 64A010A[20] airfoil coordinates) are in reasonable agreement with HYTRAN2 and EXTRAN2 for $M<0.82$. Multiple flutter points are predicted by OPTRAN2 for Mach numbers above the minimum M_f ($0.85<M<0.87$) and the HYTRAN2 calculations have confirmed this effect at $M=0.875$. Reference 30 indicates a complex flutter boundary at larger values of V for $0.88<M<0.90$ which has not been studied with HYTRAN2. Thus the flutter boundary between $M=0.875$ and 0.9 is not shown. For $M\geq 0.9$ the shock has moved off the trailing edge and the EXTRAN2 and HYTRAN2 results are in good agreement.

Table 3 Modal estimates for MBB A-3 at $M=0.775$ and $\alpha=0$ deg as a function of h_0

h_0	s_1, rad/s	s_2, rad/s	a_1, deg	a_2, deg
0.01	$-1.31+j117.17$	$-46.53+j529.55$	0.28	0.34
0.02	$-1.26+j117.17$	$-46.20+j528.77$	0.60	0.66
0.04	$-1.02+j117.15$	$-46.48+j528.28$	1.21	1.31
0.10	$0.42+j117.24$	$-48.85+j527.14$	2.97	3.24

Effect of Angle of Attack

The angle of attack is known to be an important parameter affecting transonic flutter. Ashley[28] lists several instances of such an effect and Doggett and Ricketts[29] have studied the effect of angle of attack upon an arrow-wing configuration. Edwards[30] gives subcritical damping estimates indicating changes in damping ratio of 0.02 for a 0.3 deg increase in angle of attack for a supercritical wing. Yates et al.[31] give wind tunnel flutter test results of a similar wing at several different angles of attack. A novel feature of the flutter boundaries shown is the occurrence of multiple flutter speed indices for Mach numbers less than that at the bottom of the transonic dip. That is, as the flutter speed index decreased with increasing Mach number, cases were studied in which further decreases in speed index resulted in the flutter Mach number decreasing also. This curl-back of the flutter boundary occurred for angle-of-attack changes of approximately 2 deg. Houwink et al.[32] report a similar occurrence.

The effect of angle of attack upon the flutter boundaries of the NACA 64A010 and MBB A-3 airfoils are shown in Figs. 7 and 8. Changes in α of 1.5 deg can induce a 50% drop in V_f for the NACA 64A010 between Mach 0.775 and 0.80 and a 60% drop in V_f for the MBB A-3 between Mach 0.77 and 0.79. The reduced frequencies at flutter for the two examples range from $k_f\approx 0.12$ for the higher V_f values to $k_f\approx 0.2$ for the lowest. A key feature is that the boundaries of Fig. 7 show a more gradual steepening than those of Fig. 8 as Mach number increases. Comparing Figs. 5 and 8 indicates that the abrupt steepening of the MBB A-3 boundaries occurs at the Mach number at which the upper-surface shock forms. The minimum V_f of both airfoils is approximately 0.5 and is not a strong function of α. Also, the width of the transonic dip near the minimum V_f is greater for the NACA 64A010 than for the MBB A-3, which correlates with the change in Mach number required for the shock to travel from near midchord to the trailing edge (see Figs. 4 and 5). For both airfoils, the boundary rises sharply when the shock reaches the trailing edge.

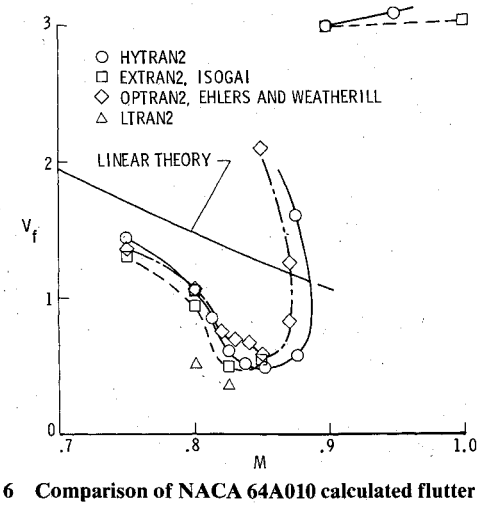

Fig. 6 Comparison of NACA 64A010 calculated flutter boundaries.

Figure 9 gives the bending mode root locus for the NACA 64A010 vs V for several angles of attack and Mach numbers. Figure 9a presents root loci typical of the case in which the shock has not yet moved aft on the airfoil (see Fig. 5). Increasing angle of attack causes a loss of damping and a drop in flutter speed index and frequency. Figure 9b typifies the case in which the shock is near the trailing edge. Minimum values of V_f occur for this condition and over a small range of angle of attack there is little effect upon damping or flutter frequency. In Fig. 9c the shock is still further aft and, for the larger values of α, has moved off of the trailing edge. In this case, the effect of increasing angle of attack reverses, with increasing damping resulting for $\alpha > 0.5$ deg. Also, the locus for $\alpha = 0.75$ deg indicates the cause of the multiple values of flutter boundaries shown in Fig. 7. None of these mechanisms appear to address the experimental condition described by Yates et al.[31] and Houwink et al.[32] in which the flutter boundary was multiple-valued for Mach numbers less than that at the bottom of the transonic dip. This observation led to the investigation described in the following section of the effect of aeroelastic twist due to the static pitching moment.

Effect of Static Pitching Moment

In Eq. (3), c_{m_o} acts as a preload which is adjusted to maintain the airfoil at a desired steady angle of attack. An alternative viewpoint is adopted in this section by introducing the wind-off angle of attack, α_o, and rewriting the static pitching moment equation as

$$k_\alpha(\alpha - \alpha_o) = \tfrac{1}{2}\rho U^2 (2b)^2 c_m(\alpha, M) \tag{11}$$

which may be reorganized as

$$V^2 = \pi r_\alpha^2 (\alpha - \alpha_o)/2c_m(\alpha, M) \tag{12}$$

Equation (12) is a nonlinear equation relating the equilibrium angle of attack, α, to the speed index, V, for given values of α_o and M. With reference to strip-theory type analyses of wings, α_o may be regarded as a "wing root angle of attack" and α as the local section angle of attack. The static pitching moment coefficient, $c_m(\alpha)$, is plotted vs α and M for the NACA 64A010 and MBB A-3 airfoils in Figs. 10 and 11. For a given Mach number, the pitching moment curves display three characteristics as α increases: 1) A range of α in which c_m varies relatively linearly with α which corresponds to the transition from shockless flow to flow with mild shocks (see Figs. 4 and 5), 2) a range of α in which c_m rises steeply corresponding to strong shocks moving aft on the airfoil, and 3) a range in which c_m again varies linearly with α with a slope which is independent of M corresponding to supersonic flow over the upper surface of the airfoil. Note particularly that the slope of the c_m curve in the first region varies gradually for the symmetrical NACA 64A010 with both M and α whereas the slope of the c_m curve for the supercritical MBB A-3 is almost independent of M and α in this region.

Figures 7 and 8 give flutter boundaries as a function of α. In order to determine flutter boundaries as a function of α_o, taking into account twisting due to the steady pitching moment, the data from Figs. 7 and 8 were crossplotted vs α for fixed M and solutions of Eq. (12) superimposed. Figure 11 gives such plots for the NACA 64A010 at $M = 0.8$ and the MBB A-3 at $M = 0.775$. Intersections of the solution of Eq. (12) for a given α_o with the flutter boundary curve represent flutter points at the indicated value of α. Figure 11a is typical for the NACA 64A010 in that only one flutter point occurs for each value of α_o. In contrast, Fig. 11b shows that the MBB A-3 has three flutter points for a range of α_o near 4 deg. This occurs due to the steeper slope of the flutter boundary curves of the MBB A-3 coupled with the pitching moment behavior shown in Fig. 10.

Figure 12 presents the effect of static pitching moment upon the flutter boundary of the two airfoils for 2 deg $< \alpha_o <$ 5 deg. Comparing Figs. 7 and 12a, the effect for the NACA 64A010 is to steepen the flutter boundaries for Mach numbers between $M = 0.75$ and 0.8. Comparing Figs. 8 and 12b, the effect for the MBB A-3 is much more pronounced. Multiple flutter points for a given Mach number cause the flutter boundary to curl back as V is decreased for $\alpha_o \geq 3$ deg. The amount of the curl-back in flutter Mach number is similar to that shown in Ref. 31. At $\alpha_o = 4$ deg, M_f decreases 0.025 as V_f decreases from 1.1 to 0.65. The flutter boundaries shown in Fig. 12 for $V_f < 0.8$ correspond to Mach number and angle-of-attack combinations in which the shock has moved aft on the airfoil. In these cases, unmodeled boundary-layer effects are probably important. Nevertheless, the similarity of the flutter boundary curl-back seen in Fig. 12b to those shown in Refs. 31 and 32 indicates that static aeroelastic twisting can have a significant effect upon transonic flutter.

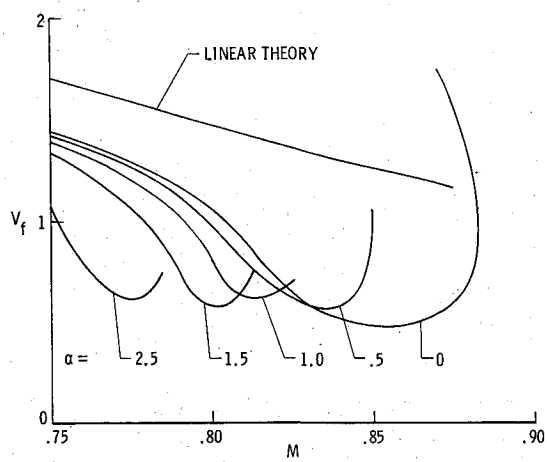

Fig. 7 Effect of angle of attack upon NACA 64A010 flutter boundaries obtained from HYTRAN2.

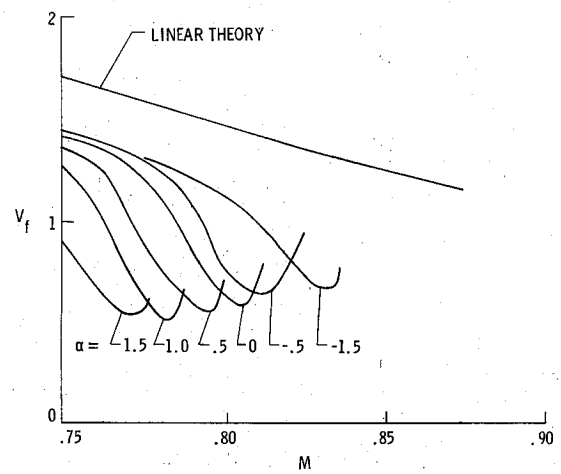

Fig. 8 Effect of angle of attack upon MBB A-3 flutter boundaries obtained from HYTRAN2.

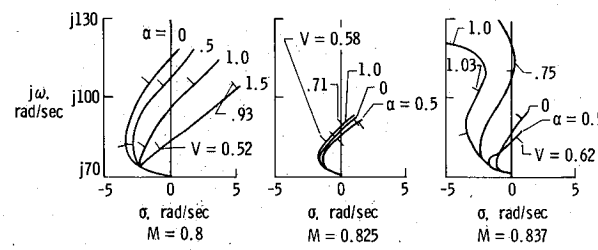

Fig. 9 NACA 64A010 flutter mode root locus as a function of M, V, and angle of attack. a) $M = 0.8$, b) $M = 0.825$, c) $M = 0.837$.

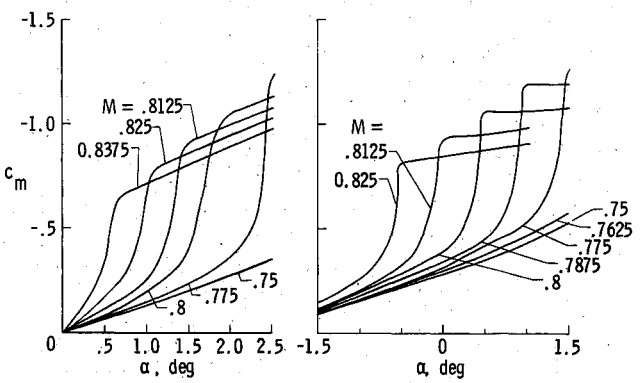

Fig. 10 Static pitching moment about $x/b=-2$ as a function of Mach number and angle of attack. a) NACA 64A010, b) MBB A-3.

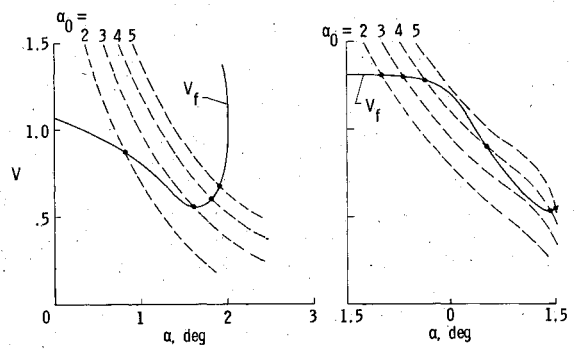

Fig. 11 Graphical determination of flutter conditions at $M=0.8$ including effect of static pitching moment. a) NACA 64A010. b) MBB A-3.

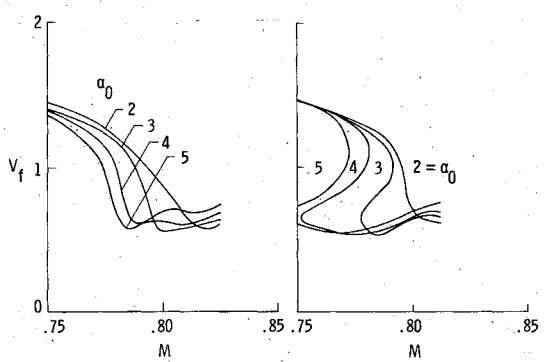

Fig. 12 The effect of static pitching moment on flutter boundaries. a) NACA 64A010, b) MBB A-3.

The multiple-valued flutter curves shown in Fig. 12b have an interesting interpretation in terms of flutter testing. At $M=0.775$ and $\alpha_o=3$ deg, the bending mode root locus as a function of speed index is shown in Fig. 13. The speed index V and actual angle of attack α are noted along the locus and show that the airfoil is twisted nose down as V is increased. Shown near $V=0.6$ and $\alpha=1$ deg is a local minimum in damping due to the proximity to the $\alpha_o=3$ deg flutter boundary shown in Fig. 12b. As V increases, the mode becomes damped again and finally flutters at $V_f\approx 1.3$ where $\alpha\approx -0.7$ deg. A small increase in either M or α_o would lead to flutter at $V_f\approx 0.6$. The flutter point at $\omega=133$ rad/s corresponds to a classical type of flutter in which significant frequency coalescence occurs. The incipient flutter condition at $\omega=85$ rad/s has much less frequency coalescence and is similar to cases which have been termed "single degree-of-freedom" or "shock induced" flutter.[28] Inspection of the static pressure distributions corresponding to these two conditions in Fig. 5 indicates that the lower-frequency flutter occurs when a shock has developed on the upper surface.

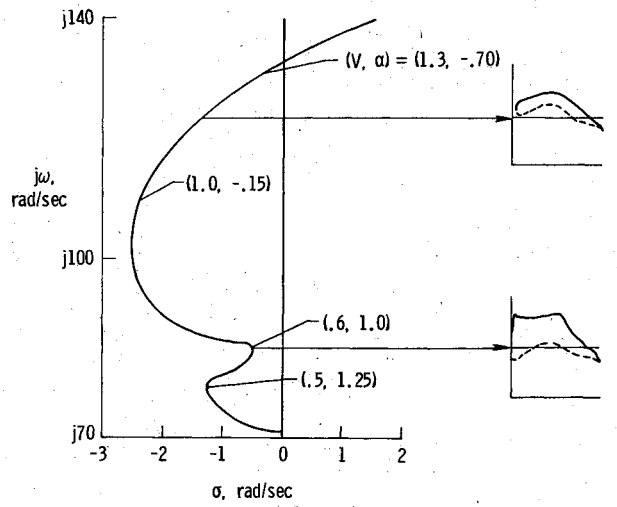

Fig. 13 MBB A-3 flutter mode root locus vs V for $\alpha_0=3$ deg and $M=0.775$.

Concluding Remarks

The transonic small perturbation equation has been coupled with the structural equations of motion of a pitching and plunging airfoil and time-marching transient flutter solutions have been obtained. Accurate frequency and damping estimates were obtained by means of a complex exponential least squares curve fit of the responses. The accuracy of the time-marching calculations was established by comparison of results from the linearized transonic equation and by comparison of the flutter boundary obtained with the nonlinear equation with published results. The preferred algorithm is a modified state transition matrix integrator which was more accurate and stable for larger time steps than the others.

The flutter boundaries of symmetrical NACA 64A010 and supercritical MBB A-3 airfoils were determined for an example demonstrating a pronounced transonic dip. Comparison of flutter boundaries calculated using several nonlinear transonic aerodynamic codes show good agreement in predicting the transonic dip. The response at flutter was surprisingly linear in amplitude for angle-of-attack oscillations of up to 3 deg. The effect of angle of attack upon the flutter boundaries of the two airfoils was determined. Changes of 1.5 deg in angle of attack can cause a 50% decrease in flutter speed index for the NACA 64A010 and a 60% decrease for the MBB A-3. The slope of the flutter boundary with Mach number is larger for the MBB A-3 airfoil and appears to correlate with steady shock strength and locations on the airfoil. When aeroelastic twisting due to the static pitching moment is included, the steeper flutter boundary of the MBB A-3 leads to the occurrence of multiple flutter points for a given Mach number and a situation in which the flutter boundary Mach number decreases as speed index is decreased. This effect has been observed in flutter model tests.

References

[1] Ballhaus, W. F. and Goorjian, P. M., "Implicit Finite-Difference Computations of Unsteady Transonic Flow About Airfoils," *AIAA Journal*, Vol. 15, Dec. 1977, pp. 1728-1735.

[2] Ballhaus, W. F. and Goorjian, P. M., "Computation of Unsteady Transonic Flows by the Indicial Method," *AIAA Journal*, Vol. 16, Feb. 1978, pp. 117-124.

[3] Rizzetta, D. P., "Time-Dependent Response of a Two-Dimensional Airfoil in Transonic Flow," *AIAA Journal*, Vol. 17, Jan. 1979, pp. 26-32.

[4] Yang, T. Y., Guruswamy, P., and Striz, A. G., "Aeroelastic Response Analysis of Two-Dimensional, Single and Two Degree of Freedom Airfoils in Low-Frequency, Small Disturbance Unsteady Transonic Flow," AFFDL-TR-79-3077, June 1979.

[5]Yang, T. Y., Guruswamy, P., and Striz, A. G., "Flutter Analysis of a Two-Dimensional and Two-Degree-of-Freedom Supercritical Airfoil in Small-Disturbance Unsteady Transonic Flow," AFWAL-TR-80-3010, March 1980.

[6]Traci, R. M., Albano, E. D., and Farr, J. L. Jr., "Perturbation Method for Transonic Flows About Oscillating Airfoils," *AIAA Journal*, Vol. 14, Sept. 1976, pp. 1258-1265.

[7]Houwink, R. and van der Vooren, J., "Improved Version of LTRAN2 for Unsteady Transonic Flow Computations," *AIAA Journal*, Vol. 18, Aug. 1980, pp. 1008-1010.

[8]Rizzetta, D. P. and Chin, W. C., "Effect of Frequency in Unsteady Transonic Flow," *AIAA Journal*, Vol. 17, July 1979, pp. 779-781.

[9]Isogai, K., "Transonic Dip Mechanism of Flutter of a Sweptback Wing: Part II," *AIAA Journal*, Vol. 19, Sept. 1981, pp. 1240-1242.

[10]Borland, C. J. and Rizzetta, D. P., "Nonlinear Transonic Flutter Analysis," *AIAA Journal*, Vol. 20, Nov. 1982, pp. 1606-1615.

[11]Engquist, B. and Osher, S., "Stable and Entropy Satisfying Approximations for Transonic Flow Calculations," *Mathematics of Computations*, Vol 34, No. 149, Jan. 1980, pp. 45-75.

[12]Edwards, J. W., Bennett, R. M., Whitlow, W. Jr., and Seidel, D. A., "Time-Marching Transonic Flutter Solutions Including Angle-of-Attack Effects," *Proceedings of the AIAA Structures, Structural Dynamics, and Materials Conference*, New Orleans, La., May 1982, pp. 220-233.

[13]Bland, S. R., "Development of Low Frequency Kernel-Function Theory and Comparison with Time-Dependent Finite-Difference Methods," NASA TM 83283, May 1982.

[14]Goorjian, P. M. and Van Buskirk, R., "Implicit Calculations of Transonic Flows Using Monotone Methods," AIAA Paper 81-0331, St. Louis, Mo., 1981.

[15]Brockett, R. W. *Finite Dimensional Linear Systems*, John Wiley and Sons, Inc., New York, 1970.

[16]Edwards, J. W., "A FORTRAN Program for the Analysis of Linear Continuous and Sampled-Data Systems," NASA TM X-56038, Jan. 1976.

[17]Isogai, K., "Numerical Study of Transonic Flutter of a Two-Dimensional Airfoil," National Aerospace Laboratory, Japan, TR-617T, July 1980.

[18]Bennett, R. M. and Desmarais, R. N., *Curve Fitting of Aeroelastic Transient Response Data with Exponential Functions in Flutter Testing Techniques*, NASA SP-415, 1975, pp. 43-58.

[19]Abbott, I. H. and von Doenhoff, A. E., *Theory of Wing Sections*, Dover Publications, Inc., N.Y., 1959.

[20]Bland, S. R., "AGARD Two-Dimensional Aeroelastic Configurations," AGARD Advisory Rept. 156, 1980.

[21]Rizzetta, D. P. and Yoshihara, H., "Computation of the Pitching Oscillation of a NACA 64A010 Airfoil in the Small Disturbance Limit," AIAA Paper 80-0128, Pasadena, Calif., Jan. 1980.

[22]Yang, T. Y., Guruswamy, P., and Striz, A. G., "Applications of Transonic Codes to Flutter Analysis of Conventional and Supercritical Airfoils," *Proceedings of the AIAA Structures, Structural Dynamics, and Materials Conference*, Atlanta, Ga., April 1981, pp. 332-342.

[23]Yang, T. Y. and Chen, C. H., "Flutter and Time Response Analysis of Three Degree of Freedom Airfoils in Transonic Flow," AFWAL-TR-81-3103, Aug. 1981.

[24]Bucciantini, G., Oggiano, M. S., and Onorato, M., "Supercritical Airfoil MBB A-3 Surface Pressure Distributions, Wake and Boundary Condition Measurements in Experimental Data Base for Computer Program Assessment," AGARD AR-138, 1979.

[25]Tijdeman, H., "Investigations of the Transonic Flow Around Oscillating Airfoils," National Aerospace Laboratory, the Netherlands, NLR TR 77090 U, 1977.

[26]Dowell, E. H., Bland, S. R., and Williams, M. H., "Linear/Nonlinear Behavior in Unsteady Transonic Aerodynamics," *Proceedings of the AIAA Dynamics Specialists Conference*, Atlanta, Ga., April 1981, pp. 654-670.

[27]Ehlers, F. E. and Weatherill, W. H., "A Harmonic Analysis Method for Unsteady Transonic Flow and Its Application to the Flutter of Airfoils," NASA CR 3537, 1982.

[28]Ashley, H., "The Role of Shocks in the 'Sub-Transonic' Flutter Phenomenon," *Journal of Aircraft*, Vol. 17, March 1980, pp. 187-197.

[29]Doggett, R. V. Jr. and Ricketts, R. H., "Effects of Angle-of-Attack and Ventral Fin on Transonic Flutter Characteristics of an Arrow-Wing Configuration," NASA TM 81914, Dec. 1980.

[30]Edwards, J. W., "Flight Test Results of an Active Flutter Suppression System Installed on a Remotely Piloted Research Vehicle," NASA TM 83132, May 1981; also, AIAA Paper 81-0655, 1981.

[31]Yates, E. C. Jr., Wynne, E. C., and Farmer, M. G., "Measured and Calculated Effects of Angle of Attack on the Transonic Flutter of a Supercritical Wing," *Proceedings of the AIAA Structures, Structural Dynamics, and Materials Conference*, New Orleans, La., May 1982, pp. 122-144.

[32]Houwink, R., Kraan, A. N., and Zwaan, R. J., "A Wind-Tunnel Study of the Flutter Characteristics of a Supercritical Wing," *Proceedings of the AIAA Dynamics Specialists Conference*, Atlanta, Ga., April 1981, pp. 748-754.